Magnetron injection gun for a broadband gyrotron backward-wave oscillator

C. P. Yuan,[1] T. H. Chang,[1,a)] N. C. Chen,[1] and Y. S. Yeh[2]
[1]*Department of Physics, National Tsing Hua University, Hsinchu 300, Taiwan*
[2]*Department of Electro-Optical Engineering, Southern Taiwan University, Tainan 710, Taiwan*

(Received 13 April 2009; accepted 7 July 2009; published online 27 July 2009)

The magnetron injection gun is capable of generating relativistic electron beam with high velocity ratio and low velocity spread for a gyrotron backward-wave oscillator (gyro-BWO). However, the velocity ratio (α) varies drastically against both the magnetic field and the beam voltage, which significantly limits the tuning bandwidth of a gyro-BWO. This study remedies this drawback by adding a variable trim field to adjust the magnetic compression ratio when changing the operating conditions. Theoretical results obtained by employing a two-dimensional electron gun code (EGUN) demonstrate a constant velocity ratio of 1.5 with a low axial velocity spread of 6% from 3.4–4.8 Tesla. These results are compared with a three-dimensional particle-tracing code (computer simulation technology, CST). The underlying physics for constant α will be discussed in depth. © *2009 American Institute of Physics*. [DOI: 10.1063/1.3187903]

I. INTRODUCTION

Gyrotrons, based on the electron cyclotron maser interaction,[1,2] are high-power, coherent, radiation sources in the millimeter/terahertz region. The gyrotron backward-wave oscillator (gyro-BWO), which features continuous frequency tunability[3] attracts more and more attention from various applications, such as electron spin resonance, plasma diagnostics, and sensitivity enhancement of nuclear magnetic resonance using dynamic nuclear polarization.[4–7]

Recently, the high efficiency and the broadband tunability of gyro-BWO were achieved at *Ka*-band[3,8] and *X*-band,[9,10] respectively. However, little literature has so far been reported at *W*-band. Due to the power handling capability, high order mode operation in gyro-BWO is requisite at such a high frequency range. A strict beam quality is demanded. The electron beam is usually generated by a magnetron injection gun (MIG)[11–13] or a cusp gun.[14,15] For the operation mode of the TE_{01},[16–19] MIG is preferred for high velocity ratio ($\alpha \equiv v_\perp / v_z$), low velocity spread ($\Delta v_z / v_z$), and easy fabrication. Unfortunately, the α declines sharply with either the increase in the magnetic field B_0 or the decrease in the beam voltage V_b, which significantly lowers the efficiency and results in narrow bandwidth.[3,8,19] Based on the above considerations, there is a pressing need to develop a MIG with high and constant α as well as low velocity spread for a *W*-band or a terahertz gyro-BWO.

In addition to B_0 and V_b, the velocity ratio is also a function of the magnetic compression ratio F_m (B_0/B_c, where B_c is the axial magnetic field at the emitter). This study proposes a variable trim field at the cathode region to adjust F_m so as to maintain the α in the tunings of V_b and B_0. A two-dimensional (2D), finite-difference method, particle tracing code (EGUN)[20] is employed for analysis. The results will be compared with a three-dimensional (3D), commercial suite-CST, Particle Studio.

a)Electronic mail: thschang@phys.nthu.edu.tw.

II. DESIGN PARAMETERS

A. General requirement for the cathode of MIG

The cathode emission loading is restricted by the cathode material and the space-charge limit. A scandate cathode will be employed to produce high current density. To ensure the lifetime, the cathode loading is better to be smaller than 15 A/cm^2 and lower than space-charge limit.[21,22] The space charge limited current density is given by Langmuir's equations.[23,24] A beam current of 6 A and a beam voltage of 70 kV are used in the simulation. To prevent the high voltage breakdown, the maximum electric field strength should be lower than 70 kV/cm at the emitter and 100 kV/cm at the entire cathode region.[21]

B. Specific requirement for *W*-band TE_{01} gyro-BWO

The MIG is designed for *W*-band gyro-BWO.[16] The operating mode is TE_{01} cylindrical waveguide mode with fundamental cyclotron harmonic ($s=1$). The waveguide radius r_w is 2.0 mm with the cutoff frequency of 91.4 GHz. The optimal magnetic field is around 38 kG with the beam voltage of 70 kV. To maximize the interacting strength, the guiding center radius (r_g) is determined from the beam-wave coupling equation,[25]

$$H_{sm}(k_{mn}r_g, k_{mn}r_L) = J_{s-m}^2(k_{mn}r_g)J_s'^2(k_{mn}r_L), \quad (1)$$

where r_g and r_L are the guiding center radius and the Larmor radius at the interaction region, respectively; $k_{mn}=x_{mn}/r_w$; J_m is the Bessel function of the first kind, and x_{mn} is the nth root of $J_m'(x)=0$. The strongest beam-wave coupling for the fundamental harmonic TE_{01} mode ($s=1$, $m=0$, and $n=1$) occurs at $r_g=0.48r_w$.[16,25] In addition, high velocity ratio is preferred to achieve high efficiency, but it is generally relative to large velocity spread ($\Delta v_z/v_z$), which significantly deteriorates the efficiency. Therefore, a moderate velocity ratio of 1.5 with a velocity spread of 6% is the design target.

 © 2009 American Institute of Physics

Author complimentary copy. Redistribution subject to AIP license or copyright, see http://php.aip.org/php/copyright.jsp

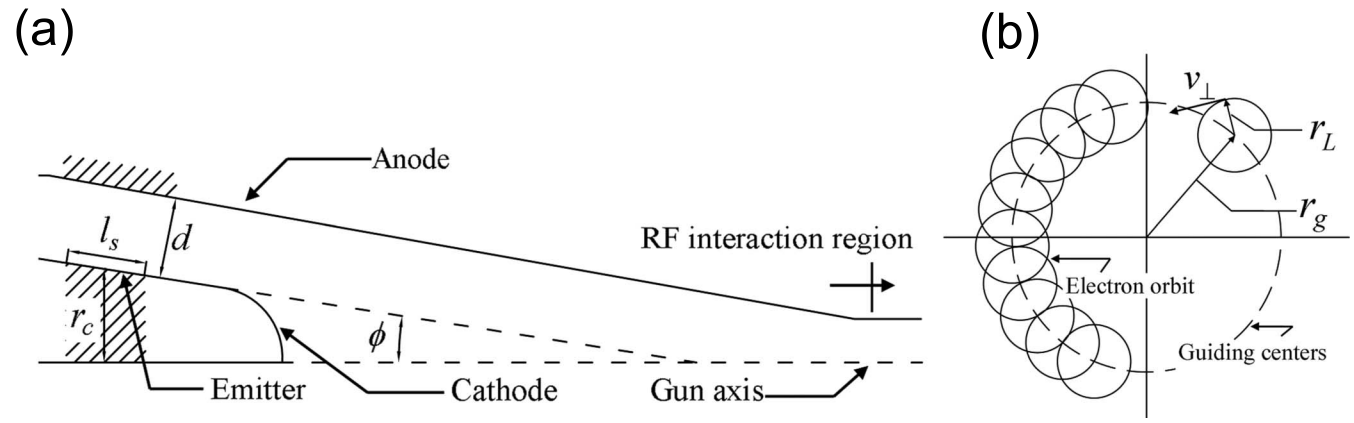

FIG. 1. (a) Schematic diagram of a single anode MIG. (b) Cross-sectional view of the electrons in the interaction region.

Figures 1(a) and 1(b) show the schematic diagram of the MIG at the cathode region and the cross-sectional view of the electron beam at the interaction region, respectively. Other variables used or shown in the figures are defined below.

J_{emis}: the emitting current density at the emitter; J_L: the space charge limited current density; l_s: the emitting length; d: the distance from the cathode to the anode; ϕ: the slope angle of the emitter; r_c: the radius of the emitter; v_z: the axial velocity at the interaction region; $v_\perp$: the transverse velocity at the interaction region; I_b: the beam current; V_b: the potential difference between the anode and the cathode.

III. DESIGN PRINCIPLES

The relations of the beam parameters, e.g., α and $\Delta v_z/v_z$ to B_0 and V_b can be derived from the first-order approximate equation of MIG.[21,26]

A. The velocity ratio

Start with the following relation:[26]

$$v_\perp \approx \frac{F_m^{3/2} E_c \cos\phi}{\gamma B_0}, \tag{2}$$

where γ is the relativistic factor $(=1+eV_b/mc^2)$; e and m are the charge and the rest mass of an electron, respectively; F_m is the magnetic compression ratio $(=B_0/B_c)$; E_c is the electric field strength at the emitter; and c is the speed of light in vacuum. Equation (2) is an approximation under adiabatic motion, which ignores the space-charge effect. Furthermore, the guiding center radius r_g should be much larger than the Larmor radius r_L and $F_m \cos^2\phi$ should be much larger than $(2\gamma v_\perp/c)^2$. These conditions are satisfied in most cases of MIG.

Since E_c, ϕ, and γ are constant in magnetic tuning, the generally trend is that the larger B_0 corresponds to the smaller $v_\perp$. Thus the velocity ratio $(\alpha \equiv v_\perp/v_z)$ decreases when B_0 increases. The relation between V_b, B_0, and α can be derived from Eq. (2) as follows:

$$\alpha = \left\{ \frac{D^2 B_0^2 c^2}{F_m^3 V_b^2 \cos^2\phi} \left[\left(1 + \frac{eV_b}{mc^2} \right)^2 - 1 \right] - 1 \right\}^{-1/2}. \tag{3}$$

The beam voltage V_b is linearly proportional to the electric field strength E_c ($V_b = DE_c$, where D is a proportional constant).

The magnetic compression ratio due to main coil is F_m $(=B_0/B_c)$. When adding a gun coil to trim the field (B_{trim}) at the emitter, the compression ratio is changed to $F_m' = B_0/(B_c + B_{trim})$. Equation (3) is modified as

$$\alpha = \left\{ \frac{D^2 B_0^2 c^2}{F_m^3 V_b^2 \cos^2\phi} \left(1 + \frac{F_m B_{trim}}{B_0} \right)^3 \left[\left(1 + \frac{eV_b}{mc^2} \right)^2 - 1 \right] - 1 \right\}^{-1/2}. \tag{4}$$

Substitute $mc^2/e \approx 511$ kV into Eq. (4) and define a handy function f,

$$f(B_0, V_b, B_{trim}) \equiv \frac{B_0^2}{V_b^2} \left(1 + \frac{F_m B_{trim}}{B_0} \right)^3 \left[\left(1 + \frac{V_b}{511} \right)^2 - 1 \right]. \tag{5}$$

Then Eq. (4) is expressed as $\alpha = [f(B_0, V_b, B_{trim})k - 1]^{-1/2}$, where k is a constant $(=D^2c^2/F_m^3 \cos^2\phi)$. The velocity ratio α will be constant, provided $f(B_0, V_b, B_{trim})$ does not change. The constant k can be determined with a known reference point (α_{ref} and f_{ref}) calculated using EGUN code. $k = (1 + \alpha_{ref}^2)/(\alpha_{ref}^2 \times f_{ref})$. For an operating condition not very far from the reference point, the velocity ratio is approximated as

$$\alpha = \left[\frac{f(B_0, V_b, B_{trim})}{f_{ref}} \left(\frac{1}{\alpha_{ref}^2} + 1 \right) - 1 \right]^{-1/2}. \tag{6}$$

Although Eq. (6) is a simplified equation and valid for adiabatic condition, the equation is useful as will be discussed later.

Author complimentary copy. Redistribution subject to AIP license or copyright, see http://php.aip.org/php/copyright.jsp

B. The velocity spread

For a gyro-BWO with broad tuning range, the velocity spread becomes critical when the operating frequency is way above the cutoff frequency. The electrons are accelerated by the beam voltage, thus all the electrons have the same kinetic energy, i.e., $v_z^2+v_\perp^2=$const. The axial and perpendicular velocity spreads are related as[27]

$$\frac{\Delta v_z}{v_z} = \alpha^2 \frac{\Delta v_\perp}{v_\perp}. \tag{7}$$

Here a minus sign is omitted because only the fluctuation amplitude matters. The electrons in the cathode emission region experience electric field and magnetic field fluctuations, which lead to the spread in the perpendicular velocity through Eq. (2). The relation is as follows:[27]

$$\frac{\Delta v_\perp}{v_\perp} = \frac{\Delta E_c}{E_c} - \frac{3}{2}\frac{\Delta B_c}{B_c}. \tag{8}$$

The perpendicular velocity spread is mostly caused by the field variations at the emitting region. The axial velocity spread can be obtained using Eqs. (7) and (8), i.e., the square of α times perpendicular velocity spread.

IV. SIMULATION SETTING

The 2D EGUN code with square mesh is used to simulate the gun properties. The coils' magnetic fields are obtained by the polynomial expansion of the axial magnetic field using ideal coils' analytic solution. The polynomial is expanded up to the sixth order of the radius.

Figure 2(a) shows the schematic diagram of EGUN simulation. A single-anode MIG is designed for the W-band TE_{01} gyro-BWO. The variable parameters are the gun position relative to the magnetic field, the emitting length l_s, the emitting angle ϕ, and the emitting ring radius r_c. For a given gun position, the magnetic compression ratio is determined. The cathode radius can be obtained from the following equation:[26]

$$B_c r_c^2 = B_0(r_g^2 - r_L^2). \tag{9}$$

The emitting length l_s is restricted by the cathode emission loading and the emitting ring radius r_c. The smaller emitting length l_s usually gives rise to the smaller velocity spread. So a minimum emitting length is chosen.

Figure 2(b) plots the magnetic field profiles for two coils: the main coil and the trim coil. The magnetic field profiles are in accord with the existing superconducting magnet at National Tsing Hua University. The magnetic field requirement for the fundamental cyclotron interaction at W-band is about 3.4–4.8 Tesla. The relative position of the emitter determines F_m, while the current of the trim coil adjusts F_m', which allows a constant α over a wide parameter space.

Figure 3 shows the simulated static electric field distribution in the cathode region when the electron beam is not present. The electric field is obtained under axial symmetric boundary condition. With this initial electric field and the magnetic field, we can calculate the electron trajectories based on the electron dynamics, which can be used to determine the charge distribution and the current density. Then, calculate the revised electric and magnetic fields. The elec-

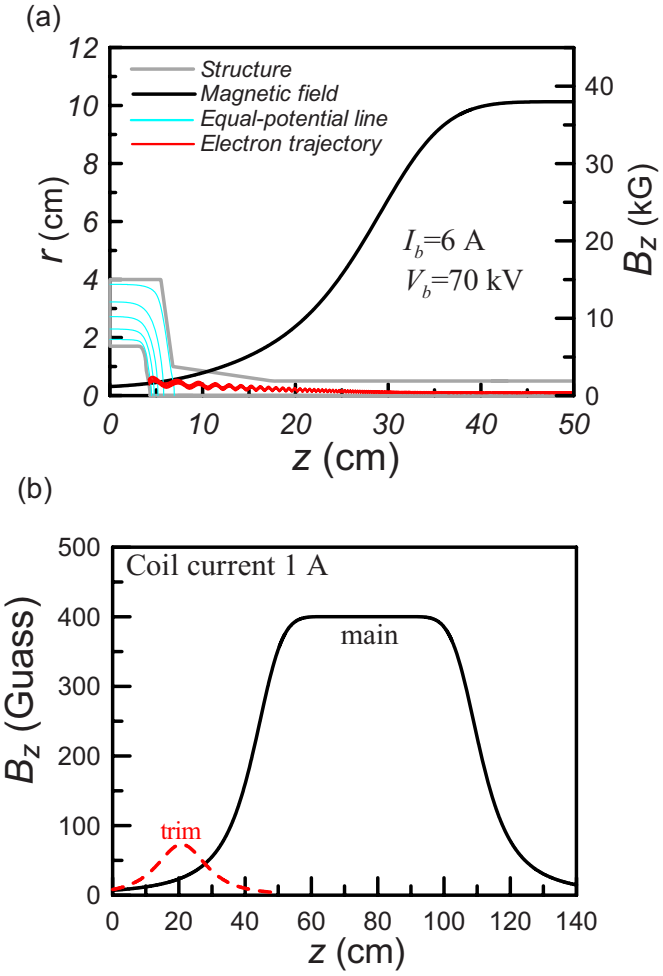

FIG. 2. (Color online) (a) Structure, electron trajectory, and axial magnetic field in EGUN simulation. (b) Axial magnetic fields of the main coil and the trim coil at a current of 1 A.

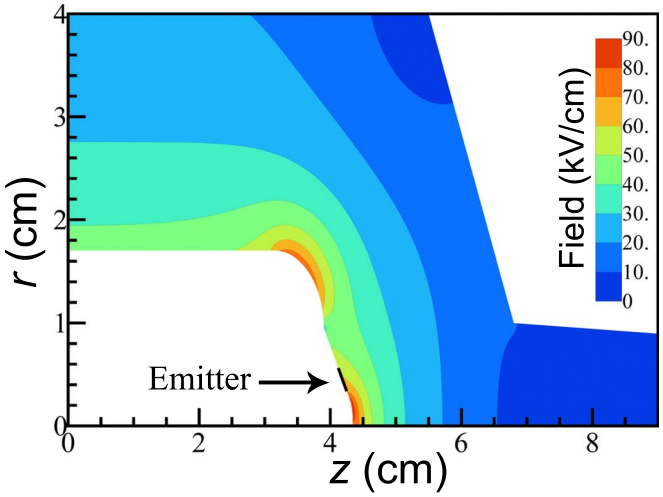

FIG. 3. (Color online) Electric field strength in EGUN simulation in the cathode region when the electron beam is not present.

Author complimentary copy. Redistribution subject to AIP license or copyright, see http://php.aip.org/php/copyright.jsp

TABLE I. Gun parameters.

Beam voltage, V_b	70 kV
Beam current, I_b	6 A
Emitting angle, ϕ	60.3°
Peak electric field	96 kV/cm
Emitting electric field	60 kV/cm
Magnetic compression ratio	23.9
Cathode radius, r_c	4.5 mm
Emitting strip length, l_s	2.3 mm
Guiding center radius, r_g	0.957 mm
Guiding center spread	11.8%
Velocity ratio, $\alpha=v_\perp/v_z$	1.51
$(\Delta v_z/v_z)_{\mathrm{EGUN}}$	3.9%
Cathode loading, J_{emis}	9.23 A/cm^2
J_{emis}/J_L	17.4%

tron trajectories and charge distribution can be solved once again. Repeat the above process until the potential is converged.

Finally, adjust the emitting angle ϕ and the geometry of the cathode to achieve the desired velocity ratio with a low velocity spread. The magnetic compression ratio (F'_m) is 23.9. Table I summarized the simulation parameters.

V. RESULTS AND DISCUSSION

Figure 4 shows the calculated α in the B_0-V_b space from Eqs. (5) and (6). The α value depends on both the magnetic field (B_0) and the beam voltage (V_b). For a magnetic field tuning with a fixed beam voltage, the value of α decreases as B_0 increases. This lowers the efficiency at high magnetic field, which limits the tuning range. The same problem occurs for the beam voltage adjustment. This is the major drawback of the "traditional" MIG and will be remedied in the following study.

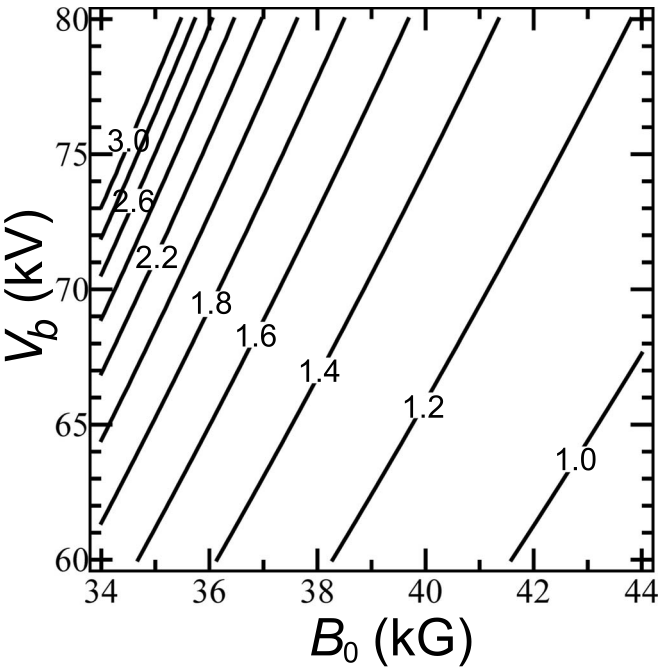

FIG. 4. Velocity ratio α vs the magnetic field B_0 and beam voltage V_b using Eqs. (5) and (6).

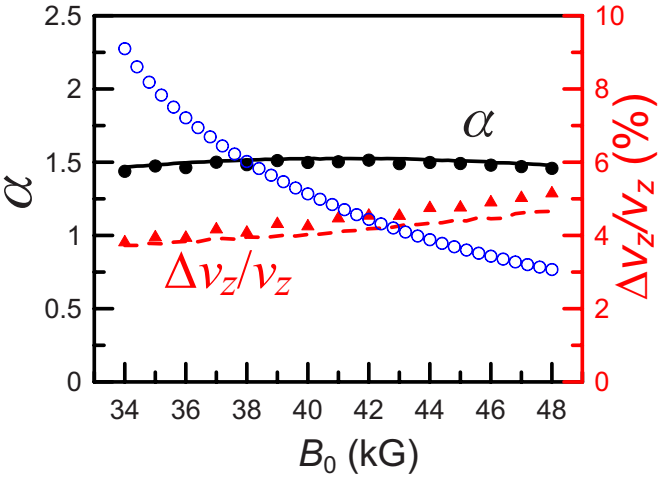

FIG. 5. (Color online) Velocity ratio α and velocity spread $(\Delta v_z/v_z)$ vs the magnetic field B_0 with a variable trim coil current [Eq. (10)]. Both EGUN (solid and dashed lines) and CST (solid dots and triangles) are presented. The open circles depict α when the trim field is not applied.

A. Magnetic field tuning

The problem of drastically changing α can be remedied by adding a trim field (B_{trim}) at the cathode to maintain a constant $f(B_0, V_b, B_{\mathrm{trim}})$, as shown in Eq. (5). The goal is to find a relation between B_0 and B_{trim} to keep f constant, since the magnetic field is linearly related to the applied current. Here is a simple equation correlating the coil currents,

$$I_{\mathrm{trim}} = -0.2451 \times I_{\mathrm{main}} + 15.53(\mathrm{A}), \tag{10}$$

where I_{trim} is the trim coil current and I_{main} is the main coil current.

Figure 5 shows the velocity ratio and axial velocity spread versus the magnetic field. The solid and dashed lines represent the velocity ratio and spread from EGUN simulations, respectively. The open circles show the velocity ratio when the trim field is not applied. The results of CST are also plotted. The solid dots and triangles show velocity ratio and spread, respectively. With the help of the variable trim field, the value of α is almost constant from 3.4 to 4.8 Tesla. The velocity spread is slightly changed, but still within the acceptable region. Basically, the results of EGUN and CST agree well.

Figure 6 shows the guiding center radius r_g as a function of the magnetic field. Both codes agree with each other in predicting the guiding center radius. Thus the following discussion will concentrate on the velocity ratio and the velocity spread only.

Author complimentary copy. Redistribution subject to AIP license or copyright, see http://php.aip.org/php/copyright.jsp

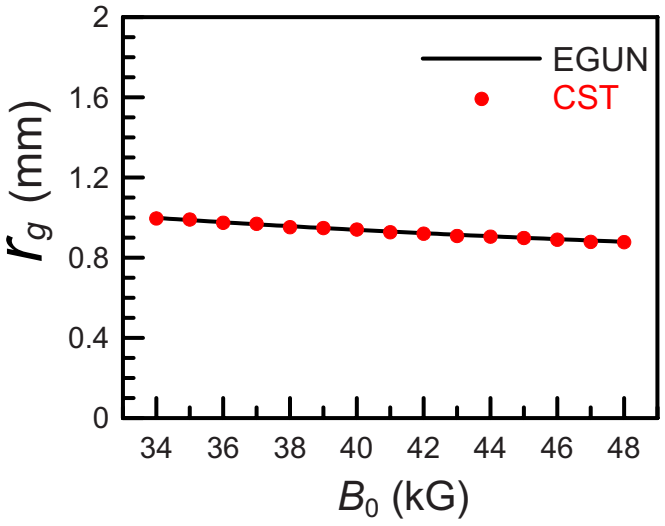

FIG. 6. (Color online) Guiding center radius r_g as a function of the magnetic field B_0 with a variable trim coil current [Eq. (10)]. EGUN's result is shown in line and CST's result is represented in solid dots. The guiding center radius (r_g) is very close to the design goal ($0.48r_w$=0.96 mm).

B. Voltage tuning

Adding a trim magnetic field (B_{trim}) can also be used to maintain a constant α during the voltage tuning. The magnetic field B_0 is 38 kG. To maintain a constant $f(B_0, V_b, B_{\text{trim}})$, here is a simple equation correlating the currents of the trim coil and the beam voltage,

$$I_{\text{trim}} = 0.115 \times V_b(\text{kV}) - 15.7(\text{A}). \tag{11}$$

Figure 7 plots the velocity ratio and the velocity spread versus the beam voltage. The solid line and dots indicate the velocity ratio with the variable trim field obtained with EGUN and CST, respectively. The open dots represent the simulated velocity ratio using EGUN with the main coil only. The dashed line and solid triangles are the velocity spread with the variable trim field using EGUN and CST, respectively. A constant α is achieved for the voltage adjustment from 60 to 80 kV. As seen in Eq. (11), the applied trim current is in the negative direction. The lower beam voltage requires a higher negative current, which raises the magnetic compression ratio to compensate the decline in α.

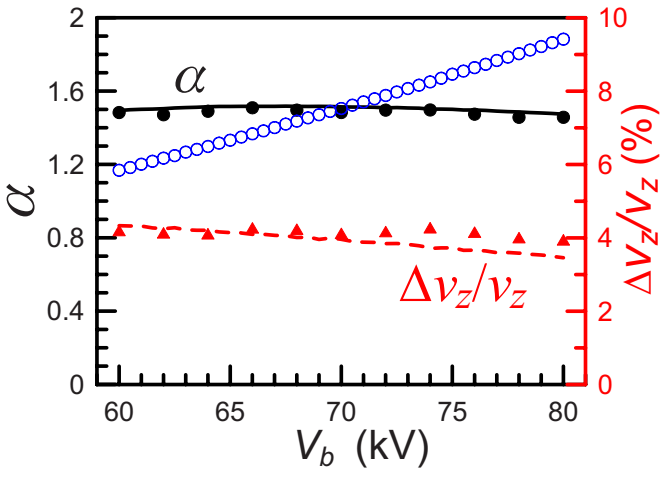

FIG. 7. (Color online) Velocity ratio α and velocity spread ($\Delta v_z/v_z$) vs the beam voltage V_b with a variable trim coil current [Eq. (11)]. Both EGUN (solid and dashed lines) and CST (solid dots and triangles) are presented. The open circles depict α when the trim field is not applied.

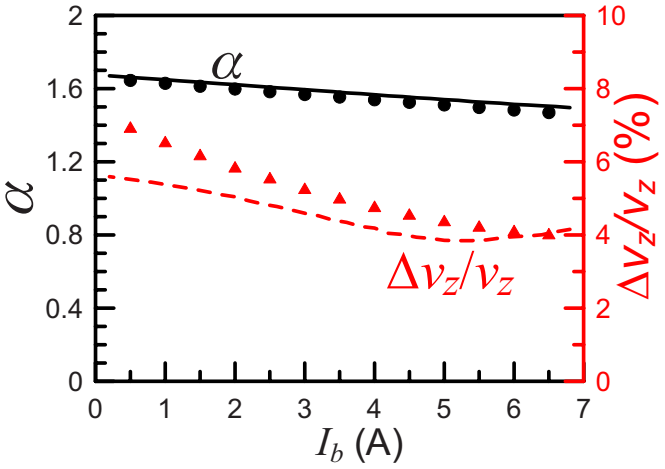

FIG. 8. (Color online) Velocity ratio α and velocity spread ($\Delta v_z/v_z$) vs the beam current I_b with a fixed trim coil current of −7.65 A. Both EGUN (solid and dashed lines) and CST (solid dots and triangles) are plotted.

C. Current tuning

Figure 8 shows the velocity ratio and the axial velocity spread as a function of the beam current for both EGUN and CST simulations. As the beam current increases, the velocity ratio decreases slightly because of the space charge effect at the emitter. The simulation results reveal that this MIG can be operated up to a maximum current of 7 A without exceeding the desired maximal velocity spread. Both codes show excellent agreement in the velocity ratio, but they have slight discrepancy in the velocity spread, especially at the low beam current. A possible reason for the discrepancy might be attributed to a large α at low beam current.

D. Velocity spread analysis

Two additional mechanisms influence the velocity spread but are not considered in the EGUN code—the effect of the cathode surface roughness and thermal effect.[28,29] Therefore, these two factors should be taken into consideration. The equations are shown in the following:

$$\left(\frac{\Delta v_\perp}{v_\perp}\right)_R = 0.4\sqrt{\frac{2eE_cR_aF_m}{\gamma m}}\frac{1}{v_\perp}, \tag{12a}$$

$$\left(\frac{\Delta v_\perp}{v_\perp}\right)_T = \sqrt{\frac{kT_cF_m}{\gamma m}}\frac{1}{v_\perp}. \tag{12b}$$

Equation (12a) is the contribution of the surface roughness, where R_a is root mean square radius of the roughness. Equation (12b) shows the thermal contribution, where T_c is the temperature at the cathode surface. Since all the factors that cause velocity spreads are statistically independent, the overall spread is the square root of the square sum as follows:

Author complimentary copy. Redistribution subject to AIP license or copyright, see http://php.aip.org/php/copyright.jsp

TABLE II. Simulated velocity spread (EGUN) and the velocity spreads caused by the surface roughness (R_a) and the thermal effect (T_c) (Ref. 30).

$(\Delta v_z/v_z)_{\mathrm{EGUN}}$	3.9%
$(\Delta v_z/v_z)_R$ at $R_a=0.8$ μm	4.3%
$(\Delta v_z/v_z)_T$ at $T_c=1200$ K	1.1%
$(\Delta v_z/v_z)_{\mathrm{Total}}$	6%

$$\left(\frac{\Delta v_z}{v_z}\right)_{\mathrm{Total}} = \sqrt{\left(\frac{\Delta v_z}{v_z}\right)^2_{\mathrm{EGUN}} + \left(\frac{\Delta v_z}{v_z}\right)^2_{R} + \left(\frac{\Delta v_z}{v_z}\right)^2_{T}}. \quad (13)$$

Table II lists the velocity spreads from the three mechanisms. The surface roughness and the temperature effect are critical as compared with the EGUN simulation. The relation between the axial and perpendicular velocity spreads can be found in Eq. (7). As seen in Table II, the overall axial velocity spread of 6% is good enough for gyro-BWO but it can be further reduced, provided the surface roughness and operating temperature are lowered.

VI. CONCLUSION

This paper reports a MIG design with the advantage of constant α over broad parameter space spanned by B_0, V_b, and I_b. It is achieved by applying a variable trim field at the cathode region. The current of the trim coil (I_{trim}) is related to B_0 and V_b. This design is for the W-band TE_{01} gyro-BWO and the idea can be applied to other devices where changing the operating parameters is needed. The simulation is conducted using EGUN code (2D) and the results are verified with CST code (3D). This MIG should enable us to develop broadband, terahertz gyro-BWO.

ACKNOWLEDGMENTS

The authors would like to acknowledge NMG Taiwan and CST for the support of CST STUDIO SUITE 2008 in the simulation. The authors are also deeply appreciative of Dr. C. F. Yu's help in the EGUN simulation. This work is sponsored by the National Science Council of Taiwan under the Contract No. NSC95-2112-M-007-035.

[1] K. R. Chu, Rev. Mod. Phys. **76**, 489 (2004).
[2] G. S. Nusinovich, *Introduction to the Physics of Gyrotrons* (The John Hopkins University Press, Baltimore, 2004).
[3] T. H. Chang, C. T. Fan, K. F. Pao, K. R. Chu, and S. H. Chen, Appl. Phys. Lett. **90**, 191501 (2007).
[4] L. R. Becerra, G. J. Gerfen, R. J. Temkin, D. J. Singel, and R. G. Griffin, Phys. Rev. Lett. **71**, 3561 (1993).
[5] C. D. Joye, R. G. Griffin, M. K. Hornstein, K. N. Hu, K. E. Kreischer, M. Rosay, M. A. Shapiro, J. R. Sirigiri, R. J. Temkin, and P. P. Woskov, IEEE Trans. Plasma Sci. **34**, 518 (2006).
[6] T. Idehara, I. Ogawa, L. Agusu, T. Kanemaki, S. Mitsudo, T. Saito, T. Fujiwara, and H. Takahashi, Int. J. Infrared Millim. Waves **28**, 433 (2007).
[7] L. Agusu, T. Idehara, I. Ogawa, T. Saito, T. Kanemaki, H. Takahashi, and T. Fujiwara, Int. J. Infrared Millim. Waves **28**, 499 (2007).
[8] C. T. Fan, T. H. Chang, K. F. Pao, K. R. Chu, and S. H. Chen, Phys. Plasmas **14**, 093102 (2007).
[9] W. He, A. W. Cross, A. D. R. Phelps, K. Ronald, C. G. Whyte, S. V. Samsonov, V. L. Bratman, and G. G. Denisov, Appl. Phys. Lett. **89**, 091504 (2006).
[10] W. He, K. Ronald, A. R. Young, A. W. Cross, A. D. R. Phelps, C. G. Whyte, E. G. Rafferty, J. Thomson, C. W. Robertson, D. C. Speirs, S. V. Samsonov, V. L. Bratman, and G. G. Denisov, IEEE Trans. Electron Devices **52**, 839 (2005).
[11] J. L. Seftor, A. T. Drobot, and K. R. Chu, IEEE Trans. Electron Devices **26**, 1609 (1979).
[12] W. Lawson, J. Calame, V. L. Granatstein, G. S. Park, C. D. Striffler, and J. Neilson, Int. J. Electron. **61**, 969 (1986).
[13] A. N. Kuftin, V. K. Lygin, Sh. E. Tsimring, and V. E. Zapevalov, Int. J. Electron. **72**, 1145 (1992).
[14] M. J. Rhee and W. W. Destler, Phys. Fluids **17**, 1574 (1974).
[15] W. He, C. G. Whyte, E. G. Rafferty, A. W. Cross, A. D. R. Phelps, K. Ronald, A. R. Young, C. W. Robertson, D. C. Speirs, and D. H. Rowlands, Appl. Phys. Lett. **93**, 121501 (2008).
[16] T. H. Chang, C. F. Yu, C. L. Hung, Y. S. Yeh, M. C. Hsiao, and Y. Y. Shin, Phys. Plasmas **15**, 073105 (2008).
[17] K. T. Nguyen, B. G. Danly, B. Levush, M. Blank, R. True, G. R. Good, T. A. Hargreaves, K. Felch, and P. Borchard, IEEE Trans. Plasma Sci. **26**, 799 (1998).
[18] H. H. Song, D. B. McDermott, Y. Hirata, L. R. Barnett, C. W. Domier, H. L. Hsu, T. H. Chang, W. C. Tsai, K. R. Chu, and N. C. Luhmann, Phys. Plasmas **11**, 2935 (2004).
[19] N. C. Chen, C. F. Yu, C. P. Yuan, and T. H. Chang, Appl. Phys. Lett. **94**, 101501 (2009).
[20] W. B. Herrmannsfeldt, SLAC, Stanford, CA, Report No. 226, 1979.
[21] W. Lawson, IEEE Trans. Plasma Sci. **16**, 290 (1988).
[22] W. Lawson and V. Specht, IEEE Trans. Electron Devices **40**, 1322 (1993).
[23] I. Langmuir and K. B. Blodgett, Phys. Rev. **22**, 347 (1923).
[24] E. W. V. Acton, J. Electron. Control **3**, 203 (1957).
[25] K. R. Chu, Phys. Fluids **21**, 2354 (1978).
[26] J. M. Baird and W. Lawson, Int. J. Electron. **61**, 953 (1986).
[27] A. V. Gaponov, V. A. Flyagin, A. L. Gol'Denberg, G. S. Nusinovich, Sh. E. Tsimring, V. G. Usov, and S. N. Vlasov, Int. J. Electron. **51**, 277 (1981).
[28] S. E. Tsimring, Radiophys. Quantum Electron. **15**, 952 (1972).
[29] Y. Y. Lau, J. Appl. Phys. **61**, 36 (1987).
[30] A. W. Fliflet, A. J. Dudas, M. E. Read, and J. M. Baird, Int. J. Electron. **53**, 743 (1982).

Author complimentary copy. Redistribution subject to AIP license or copyright, see http://php.aip.org/php/copyright.jsp